Hydrolysis-induced morphology evolution of linear and bottlebrush block copolymers in thin films with acid vapor or photoacid generators

Authors

Mingqiu Hu, Xindi Li, Javid Rzayev, Thomas P. Russell

Abstract

The self-assembly of high-χ low-*N* block copolymers (BCPs) can give patterns in thin films with sub-10 nm full pitch, serving as a promising alternative to photolithographic methods. In this work, we synthesized poly(solketal methacrylate)-block-polystyrene copolymers, PS-*b*-PSM, with various volume ratios of the two blocks. After hydrolysis of the PSM block into poly(glycerol monomethacrylate), PGM, the BCPs had both lamellar and cylindrical microdomain morphologies in the bulk phase and in thin films. In addition to our previously developed solid-state hydrolysis strategy involving trifluoroacetic acid vapors, we developed a new photo-induced solid-state hydrolysis using photoacid generator, PAGs, embedded within the polymer film. After exposure to UV followed by a post-exposure baking or solvent vapor annealing, the BCPs transitioned from the disordered, phase-mixed state into laterally ordered cylindrical patterns. In comparison to linear BCPs that rely on a random copolymer layer to modify interfacial interactions with the substrate to promote an orientation of the microdomains normal to the interrface, we found that the microdomains in bottlebrush multiblock copolymers oriented normal to the interface absent substrate modification due to the chain architecture.

Introduction

Moore's law predicts that the number of transistors in an integrated circuit doubles approximately every two years.[1] In the most advanced commercially available process, the feature size of transistors remains tens of nanometers in size, limited by the resolution of photolithography, despite the use of extreme ultraviolet lithography and multi-patterning.[2] As top-down photolithography approaches the diffraction limit, bottom-up self-assembly of block copolymers (BCPs) has proven to be a promising alternate route to give patterns on the nanometers level.[3-11] Lamellar and cylindrical patterns with sub-10 nm even full pitch have been reported.[12-20] The feasibility of integrating BCP self-assembly into the fabrication of critical device layers has been verified at the 7-nm process of fin field-effect transistors.[21-24]

BCPs can either be in their disordered state or microphase-separated state, depending on the product of the segmental interaction parameter (χ), which increases with the incompatibility of two blocks, and the degree of polymerization (*N*).[25-28] In the strong-segregation limit (large χN), the full pitch of microphase-separated lamellar morphologies is proportional $\chi^{1/6}N^{2/3}$.[12, 29] As a result, to keep the BCPs in their strong segregation limit while minimizing the full pitch, χ must be high while *N* must be low.[30-32] High-χ low-*N* BCPs usually have one hydrophobic block and one hydrophilic block, inevitably leading to poor solubility and, therefore, non-uniform films, syntheses that are more complex, and microdomain orientation that

is difficult to control, and self-assembly procsse that are difficult to direct. We developed a solid-state hydrolysis strategy to bypass the solubility issue, allowing the preparation of uniform thin films by spin coating high- χ low-N BCP precursors.[33] A hydrophobic-hydrophobic BCP, poly(solketal methacrylate)-block-polystyrene (PSM-*b*-PS), was synthesized and spin-coated into a uniform thin film. The film was then exposed to trifluoracetic acid (TFA) vapor to convert the hydrophobic PSM block into hydrophilic poly(glycerol monomethacrylate) (PGM), massively increasing χ and transitioning the BCP from the disordered, phase-mixed state into the strongly microphase-separated state. For microphase-separated BCPs, different morphologies, such as lamellar, cylindrical, gyroid, and spherical morphologies, can be achieved by tuning the volume fractions of the two blocks.[25] In our previous work, we showed the self-assembled lamellar morphologies in the bulk and in thin films.[33] In this work, we expanded the morphologies to hexagonally packed cylinders by tuning the volume fraction of the blocks of the high-χ low-*N* BCPs.

TFA is highly corrosive and, therefore, incompatible with most metallic and oxide materials used in device layers. It is, also, difficult to control the spatial exposure of the film with acid vapors, making it difficult to control a selective hydrolysis of the film. TFA is also not environmentally friendly, being non-degradable and toxic to aquatic life.[34] In this work, we replaced TFA vapor by embedding photoacid generators (PAGs) into the BCP thin films. PAGs release acid upon exposure to UV light. Therefore, by co-dissolving the PAGs with the BCPs in the solution for spin coating, a solid-state hydrolysis could affected by exposing the film to UV light followed by post-exposure baking or solvent vapor annealing. Compared with the previously developed TFA-induced hydrolysis, the photo-induced hydrolysis in this work opened possibilities for lithography-like areal-selective exposure that could be used to generate devices with sub-10 nm full pitch.

In addition to minimizing the full pitch by transforming the BCPs into the very strong-segregation regime, PS-b-PSM is soluble in a single common solvent, like toluene, allowing a simple spin-coating process to generate very uniform thin films, while the PAG eliminates the need of TFA or other strong acid vapors. However, the orientation of self-assemble microdomains must also be carefully controlled.[35-41] For high-χ low *N* BCPs, one block will preferentially interact with the substrate, promoting an orientation of the microdomains parallel to the substrate. While this is suitable for a pattern transfer of line patterns from cylindrical microdomains, it is more desirable to orient lamellar microdomains normal to the surface to enhance pattern transfer of a line pattern or, in the case of cylindrical microdomains, the transfer of a dot pattern. For linear BCPs, a random copolymer layer can be used to balance the interfacial interactions between the two blocks and the substrate, thereby promoting orientation an orientation of the microdomains normal to the surface.[33] For a solid state conversion of linear diblock copolymers, a precursor random copolymer of P(S-*r*-SM) can be used that is simultaneously converted into a random P(S-r-GM) copolymer to control the orientation of the microdomains. One can also take advantage of the chain architecture to control the microdomains orientation. Recently, bottlebrush copolymers have found use in a wide range of applications.[42, 43] Bottlebrush block copolymers have been shown to produce

microdomains oriented normal to the substrate interface absent any substrate modification despite the preferential interactions of one block with the substrate due to the architecture of the polymer chain and a maximization of contact of one block with the substrate.[44, 45] With increasing χ and an even stronger preferential interaction of one block with the substrate, as is the case for the S and GM segments with χ as high as 0.438 at 25 °C using 118 Å^3 as a reference volume[46], this architectural effect can be used to even greater advantage to orient the microdomains normal to the substrate interface absent any surface modification.

Experimental Section

Materials

Dioxane, toluene, hydrochloric acid, trifluoroacetic acid, and the two photoacid generators were purchased from Sigma-Aldric. and used directly without purification. The block copolymers were synthesized using a previously developed synthesis route.[47, 48] Kapton tape for transmission x-ray scattering measurements was purchased from Fisher Scientific. Silicon wafers were purchased from International Wafer Service, Inc. (IWS). The polished side of Si wafers has a natural SiO_2 layer.

Hydrolysis of the BCPs in solution

The BCPs were dissolved in dioxane at 20 mg/mL. Next, concentrated hydrochloric acid was diluted to 1 M, and 5% by volume was added to the BCP solution, stirred at room temperature for 12 hours, frozen with liquid nitrogen, and dried in a vacuum oven.

Hydrolysis of the BCPs in thin films with TFA vapor

Silicon wafers with a natural top SiO_2 layer were cut into 1*1 cm^2 pieces, cleaned with a CO_2 snow jet, then ozone plasma for 20 minutes. In some experiments, the Si wafers were modified with a random copolymer layer with our previously developed strategy.[33] The BCPs were dissolved in toluene solution at 20 mg/mL. Next, 40 µL solution was dropped on a wafer immediately followed by spin-coating at 6000 rpm for 1 minute. The polymer films were then placed in a glass jar saturated with TFA acid vapor, arising from a mixture of TFA and water at a volume ratio of 3/1. After 2-4 hours, the films were removed from the jar and evacuated, followed by thermal annealing at 150 °C for 12 hours.

Hydrolysis of the BCPs in thin films with photoacid generators

Silicon wafers were cleaned and modified in the same way as mentioned above. BCPs and PAGs were dissolved in toluene solution at 20 mg/mL and 0.1 mg/mL. 40 µL solution was dropped on a wafer immediately followed by spin-coating at 6000 rpm for 1 minute. For PAG1, the film was exposed to 360 nm UV light. For PAG2, the film was exposed to 254 nm UV light. The dose of exposure was 50 mJ/cm^2. After exposure, there were two different routes to proceed with the acid-catalyzed hydrolysis reaction and morphology evolution. For post-exposure baking followed by thermal annealing, the films after exposure to UV light were firstly baked at 100 °C

in the air and then moved into a vacuum oven for thermal annealing at 150 °C for 12 hours. For solvent vapor annealing, the films after exposure were placed in a glass jar saturated with toluene and water vapor for 19.5 hours.

Small-angle x-ray scattering (SAXS) and grazing-incidence small-angle x-ray scattering (GISAXS) of the BCPs hydrolyzed in solution

A steel washer with a thickness of 0.5 mm was placed on top of a Kapton tape and heated to 100 °C. After hydrolysis in dioxane solution and vacuum drying, the BCP powders were compressed into the washer. Another Kapton tape was placed on top of the steel washer to sandwich the BCPs between two Kapton films in a washer. The samples were thermally annealed at 150 °C for 12 hours before SAXS measurements. The x-ray scattering facility is a Ganesha SAXS-LAB instrument. The x-ray source is Cu K_α with a wavelength of 0.1542 nm. The collimation system has two sets of apertures, each comprising a horizontal and a vertical gate to control the beam size. The detector is a Pilatus 300K 2D detector with a beam stop in the center to measure the 2D scattering profile, which can be converted into a 1D scattering profile after the azimuthal average. The beam stop can be removed to measure the incident beam intensity. All measurements were performed in vacuum for 10 minutes. GISAXS measurements were performed at an incidence angle of 0.18 degrees.

Surface characterization

Atomic force microscopy was performed on an Asylum MFP-3D under tapping mode. The AFM probes were purchased from Bruker. The model of the probe is NCHV. The normalized radius of the tip is 8 nm. Reactive ion etching was performed on an STS Vision 320 Mark II RIE System with RF power 100 W under 10 mTorr for 15 seconds. The gas used for RIE is a mixture of O_2 and Ar at a 3/1 volume ratio. SEM experiments were performed using an FEI Magellan XHR-400 field emission-SEM operated at 1 kV acceleration voltage and 50 pA beam current.

X-ray reflectivity measurements (need to discuss how to publish experimental details, maybe patentable?)

Results and Discussion

In this work, we synthesized PSM-*b*-PS using a previously developed synthesis.[47] The chemical structure of the block copolymer is shown in Scheme 1a. Solid-state hydrolysis of PSM into PGM in spin-coated thin films was achieved by a previously used TFA vapor strategy and a newly developed PAG route. Hydrolysis in solution could was achieved with hydrochloric acid.[49] Before hydrolysis, the segmental interaction parameter (χ) between the two blocks was low, 0.035 at 25 °C using 118 Å^3 as a reference volume.[46] As a result, the BCPs were in the disordered state. Uniform thin films of PS-b-PSM, ~50 nm in thickness, were spin-coated from solutions of PS-*b*-PSM in toluene.[33] After hydrolysis, the BCPs changed from hydrophobic-hydrophobic BCPs into hydrophilic-hydrophobic BCPs with significantly increased χ, 0.438 at 25 °C using 118 Å^3 as a reference volume.[46] As a result, the BCPs transitioned from a disordered, phase-mixedmorphlogy into a strongly

microphase separated morphology (Scheme 1b). We previously showed that the solid-state hydrolysis strategy yielded well-ordered lamellar microdomain morphologies in thin films.[33] Here, we found that by changing the volume ratios between the PS and PSM blocks, lamellar and cylindrical morphologies with parallel and perpendicular orientations could be achieved upon hydrolysis (Scheme 1b). While linear BCPs rely on a random copolymer layer on the substrate to promote perpendicularly oriented patterns, we found that bottlebrush multiblock copolymers exhibited perpendicularly oriented patterns without surface modification.

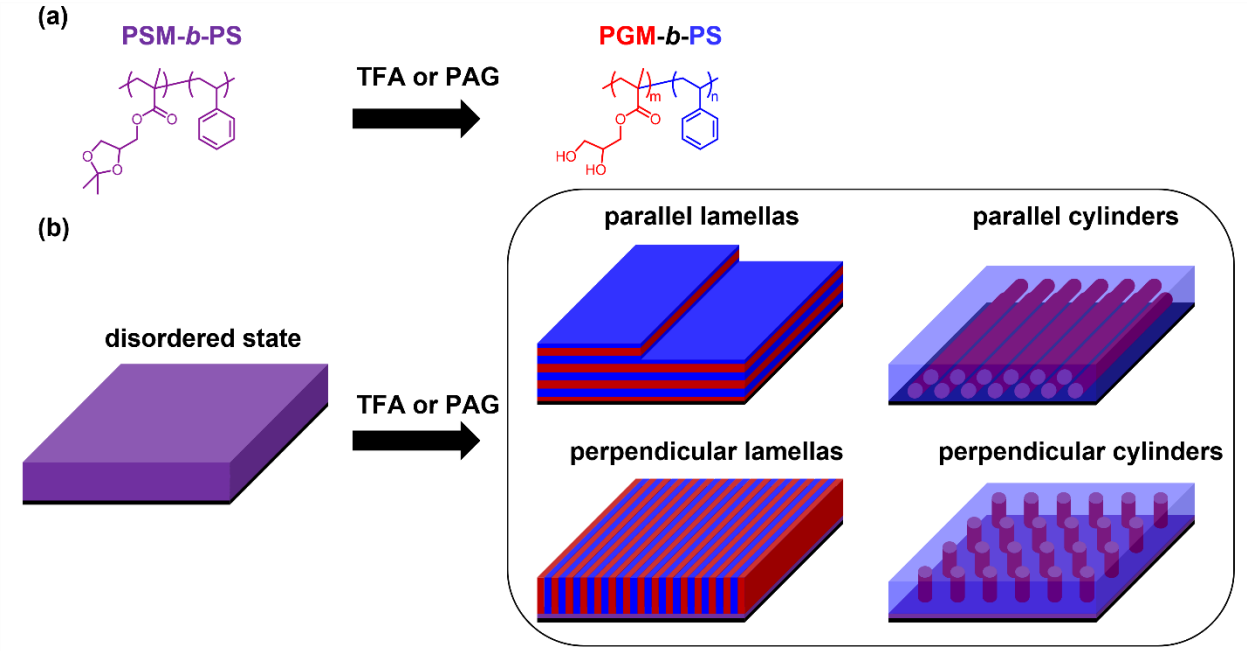

Scheme 1. (a) Solid-state hydrolysis from disordered poly(solketal methacrylate)-b-polystyrene (PSM-b-PS) into microphase-separated poly(glycerol monomethacrylate)-b-polystyrene (PGM-b-PS). The hydrolysis reaction was either catalyzed by trifluoracetic acid (TFA) or embedding photoacid generators (PAG) into the polymer film. **(b)** Morphology evolution in thin films from a disordered state before hydrolysis into lamellas or cylinders oriented parallel or perpendicular to the substrate after hydrolysis. A random copolymer layer of PSM and PS was spin-coated on the silicon substrate before the BCP layer to promote perpendicular orientation, as shown by the pink layer in perpendicularly oriented lamellae and cylinders.

The bulk morphologies of the BCPs after hydrolysis were first examined using transmission small-angle x-ray scattering (SAXS) as shown in Figure 1. The hydrolysis reaction in the dioxane solution was catalyzed by hydrochloric acid (HCl). The PGM-*b*-PS after hydrolysis was thermally annealed at 150 °C, above the glass transition temperatures of PGM (100 °C) and PS (96 °C),[46] to enhance the lateral order of the self-assembled morphologies. As the minority block, when the PGM volume fraction was gretaer than 0.32, the BCPs had lamellar morphologies, as evidenced by the primary reflection (q^*) and higher-order reflections at $2q^*$, $3q^*$, $4q^*$, and $5q^*$ in Figure 1a. The lamellar repeat period or full pitch (L_0) was calculated

by $L_0 = 2\pi/q^*$. When the volume fraction of PGM was less than 0.24, most of the BCPs ordered into hexagonally packed cylinders, as evidenced by the primary reflection (q^*) and higher-order reflections at $\sqrt{3}q^*$, $2q^*$, $\sqrt{7}q^*$, and $3q^*$ in Figure 1b. The absence of specific peaks in cylindrical morphologies, for example, 2q* for P(GM2.6-S6.3), resulted from a symmetry where a minimum of the form factor overlaps with a maximum of the structure factor. For P(GM2.6-S6.3), the minority PGM blocks formed cylinders in a PS matrix. With L_0 = 15.6 nm and a 0.23 PGM volume fraction, the radius of the PGM cylinders is estimated to be 4.5 nm. The form factor of such cylinders has a minimum at 0.85 nm^{-1}, which is close to $2q^*$ (0.81 nm^{-1}), causing the absence of the reflection at $2q^*$.[50, 51] P(GM0.9-S3.4), which showed a broad primary reflection and no higher-order reflections, was in the disordered state, since at increasing asymmetry and decreasing degree of polymerization, a larger χ is needed to be microphase separated.

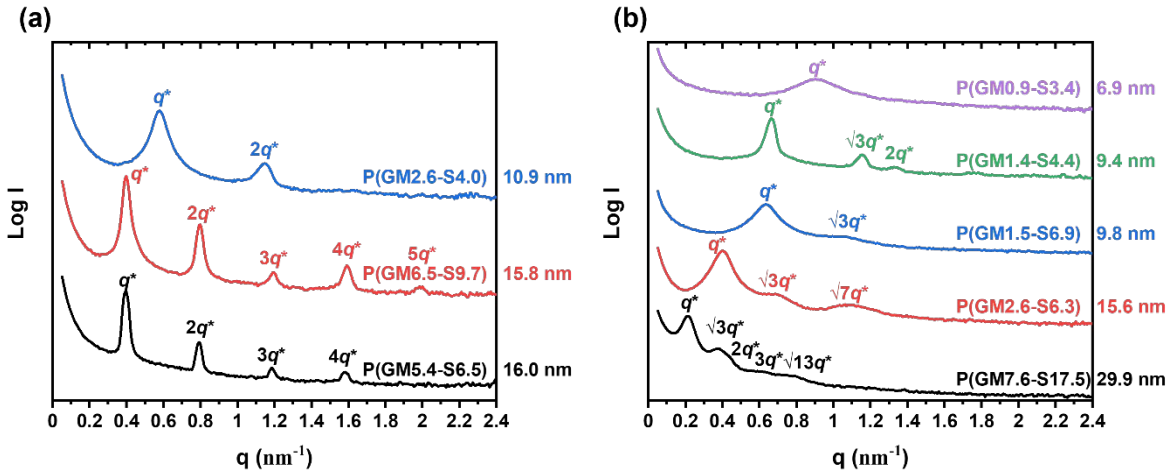

Figure 1. SAXS plot of PGM-*b*-PS block copolymers with different molecular weights after hydrolysis in solution, showing lamellar **(a)** and cylindrical **(b)** morphologies. The scattering intensity (I) is shown as a function of the scattering vector (q) and vertically shifted for clarity. The full pitch (L_0) of the morphologies was noted on the right of the plots.

The thin film self-assembly of BCPs with lamellae oriented parallel to the substrate was examined by X-ray reflectivity[52-54] (XRR, Figure 2) and AFM (Figure 3a). The BCP thin film was prepared by spin-coating, then exposed to TFA vapor, and thermally annealed at 150 °C. Si substrates with native SiO_2 surface layers (1-2 nm) were treated with UV/Ozone prior to spin coating, to remove any adsorbed organics leaving a hydrophilic surface that favored interactions with the hydrophilic PGM blocks, promoting a parallel orientation of the lamellae. As a result, P(GM6.5-S9.5) on the Si substrate showed an island-hole morphology (Figure 3a), indicating lamellae oriented parallel to the substrate. XRR of the spin-coated thin film before exposing to TFA, after exposing to TFA before thermal annealing, and after thermal annealing are shown in Figure 2. The film thickness before exposure to TFA was 467 Å. After exposure to TFA for 2 hours, the thickness decreased to 442 Å due to the loss of acetone, a by-product of the hydrolysis reaction. Exposing to TFA for 3.5

hours gave a film thickness close to the one after 2 hours, indicating that the hydrolysis was complete within 2 hours (Figurer S1). After thermal annealing, the film thickness further decreased to 429 Å. The decrease indicated that the films remained swollen after TFA and acetone rapidly evaporated. Subsequently, densification occurred during the thermal annealing above the glass transition temperatures. Before hydrolysis, the XRR profile could be fit with a simple monolayer model with diffuse interfacial profiles at the polymer-air and polymer-Si interfaces (Figure S2-3). However, after thermal annealing, the XRR profiles showed a frequency beating in the Kiessig fringes, which could not be fit a with simple monolayer model (Figure S4), but rather a coherent addition of two films with thicknesses corrrespnding to the island and hole topography. The heights of the islands, 16 nm, could be measured by a line cut in the AFM height image (Figure S5a), which was close to the full pitch obtained from bulk phase x-ray scattering (15.8 nm). In the AFM phase image (Figure S5b), the islands and the surrounding area had the same phase, indicating the same block on the top surface in those areas.

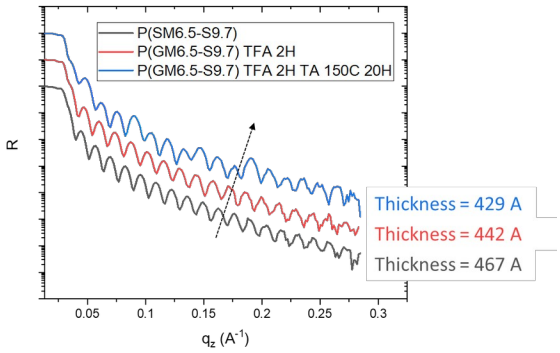

Figure 2. X-ray specular reflectivity (R) of a spin-coated P(SM6.5-S9.7) thin film on top of a silicon wafer, as a function of q_z, the difference between the reflected and incident wave vectors. The black line is from the polymer thin film before hydrolysis. The red line is the polymer film after hydrolysis in TFA vapor for 2 hours before thermal annealing. The blue line is for the polymer thin film after hydrolysis in TFA vapor for 2 hours and thermal annealing for 12 hours at 150 °C. The reflectivity at zero q_z is all normalized to be 1. The red and blue lines are vertically shifted by a magnitude for clarity. Thicknesses of the thin films are calculated from the Kiessig fringes.

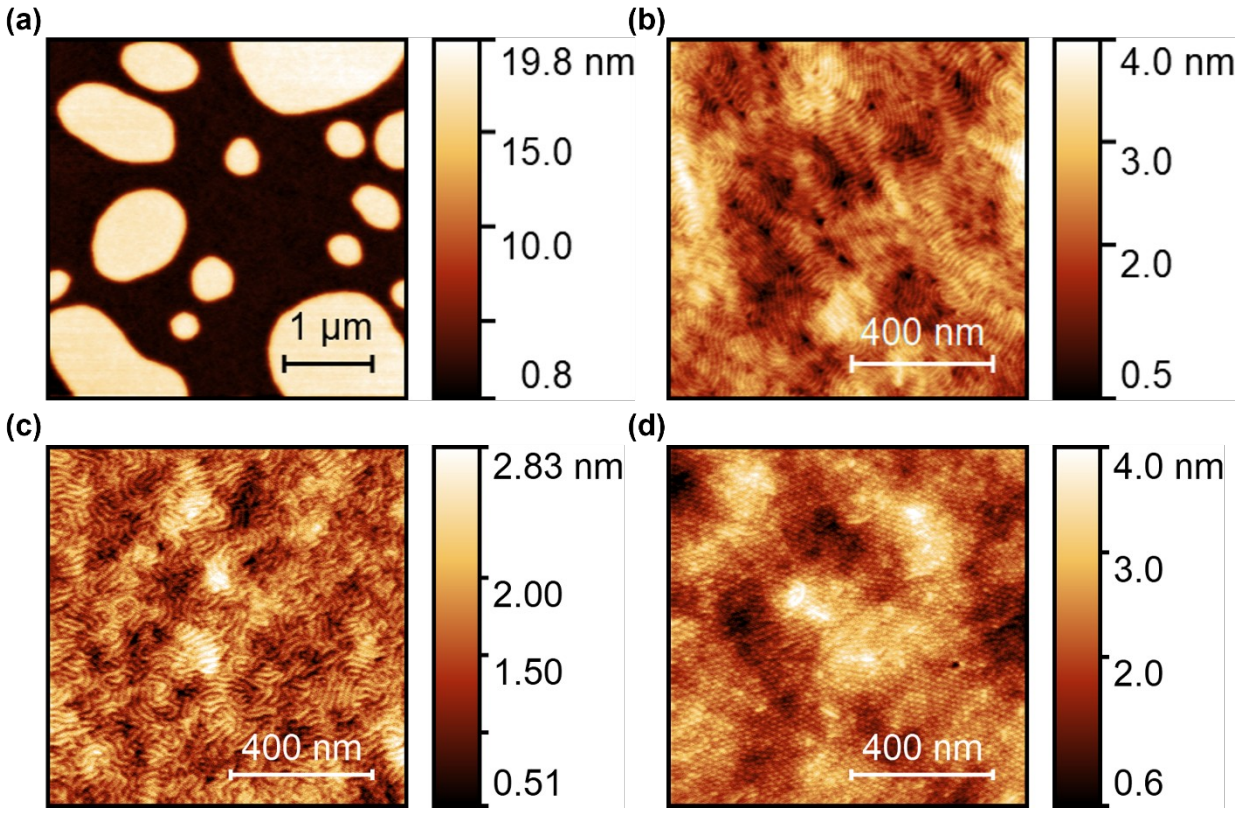

Figure 3. AFM height images of PGM-b-PS after solid-state hydrolysis with trifluoroacetic acid (TFA) vapor in thin films showing **(a)** parallel lamellae, **(b)** perpendicular lamellae, **(c)** parallel cylinders, and **(d)** perpendicular cylinders. The lamellar morphologies were from P(GM6.5-S9.7) and P(GM5.4-S6.5), and the cylindrical morphologies were from P(GM2.6-S6.3). To promote perpendicularly oriented lamellae, a random copolymer layer was used to modify the substrate prior to spin-coating the BCP layer in (b). The BCPs were spin-coated on a bare Si substrate with a natural SiO_2 top layer for the other three samples.

To obtain lamellae oriented normal to the surface (Figure 2b), a thin random copolymer layer, PSM-*r*-PS, was anchored to the substrate. Hydrolysis of PSM-*r*-PS and the PSM-*b*-PS on top of the random copolymer occurred simultaneously so that the interaction between the two blocks and the substrate remained balanced. As a result, a perpendicular orientation of the lamellae was promoted. Grazing-incidence small-angle x-ray scattering (GISAXS, Figure S6) augmentted the AFM images. Compared with AFM, which gave images of localized surface regions, GISAXS gave statistically averaged information of a much larger volume. The primary scattering reflection and higher orders were observed in the in-plane direction, suggesting a perpendicular orientation of the lamellae. Despite the well-developed lateral order, higher-order reflections were weak because the films were too thin (~ 50 nm), and the flux of the in-house x-ray source was limited. The incidence angle was set as 0.18°, close to the critical angle measured by XRR, to ensure the penetration of the x-ray into the film while maximizing the beam path to enhance the scattered intensity. Such a scattering geometry is also evidenced by comparing the relative

position of the Yoneda peak, which has the same q_z as the primary in-plane peaks, and the specular reflection at $q_y = 0$. The specular reflection had slightly higher q_z than the Yoneda band, indicating that the incidence angle was slightly above the critical angle.

P(GM2.6-S6.3) showed hexagonally packed cylinders in the bulk and thin films. Parallel and perpendicular cylinders were obtained on unmodified Si substrates (Figure 2c, 2d). After 2H hydrolysis in TFA vapor, the cylinders were oriented perpendicular to the substrate (Figure 2d). After 4H hydrolysis, the cylinders were oriented parallel to the substrate (Figure 2c). As discussed above, the hydrolysis was complete within 2H. The PGM-*b*-PS was exposed to TFA and the by-product, acetone, for an extended period of time after the hydrolysis was completed. These plasticize the copolymer film and mediate interfacial interactions, causing the orientationof the microdomains to be different tthan that observed with thermal annealing. Curiously, no apparent differences were observed in GISAXS for parallel and perpendicular oriented cylinders. Both samples showed a pair of in-plane peaks on the Yoneda band (Figure S7). The q_y of those peaks matched those of the bulk phase SAXS, confirming the hydrolysis was complete in both cases. While the in-plane GISAXS peaks were expected for the perpendicular cylinders, the parallel cylinders were expected to give peaks at 30° and 90° out-of-plane if their [100] planes were parallel to the substrate. We attribute the lack of such peaks to the absence of hexagonal packing of the parallel cylinders since the film thickness is only three full pitches. On the contrary, the hexagonal packing in a drop-cast film with micron thickness was evidenced by the peaks at 30° and 90° out-of-plane in GISAXS (Figure S8).

To replace the TFA vapor with PAG, the PAG was dissolved in toluene and mixed with the toluene solution of PSM-*b*-PS for spin coating. The film was then exposed to UV light to generate the acid (Figure 3a). Two different PAGs were chosen, one that produced HCl, abbreviated as PAG1 (Figure 3b), and one that produced a fluorinated sulfuric acid, abbreviated as PAG2 (Figure 3c). Monitoring the degree of hydrolysis of BCPs with PAG on a Si substrate is challenging by NMR because of the acid residue. Even if enough materials were dissolved for solution NMR measurements, it is difficult to determine whether the hydrolysis occurred in the solid state or the NMR solution. Consequently, we used attenuated total reflectance Fourier-transform infrared spectroscopy (FTIR) to monitor *in situ* the hydrolysis of a drop-cast film microns in thickness.[46, 55, 56] Powders of P(SM5.4-S6.5) before hydrolysis and P(GM5.4-S6.5) hydrolyzed in solution were used as a reference material s(Figure 3d). BCPs hydrolyzed with PAG1 and PAG2 exhibited a broad absorption near 3100–3600 cm^{-1} (Figure 3e-f, peak 1), like the reference, which is attributed to the stretching vibration of hydroxyl groups of glycerol monomethacrylate. This suggested that the hydrolysis reaction proceeded with PGA1 and PAG2. However, the secondary alcohol C–O stretching vibration at 1118 cm^{-1} (peak 7) is only clearly visible in the reference material, and the BCPs hydrolyzed with PAG2. For the BCPs hydrolyzed with PAG1, a flattened absorption appeared at the expected wavelength instead. This suggested that the degree of hydrolysis with PAG1 is lower than that of PAG2, possibly because HCl evaporates more readily than fluorinated sulfuric acid

during post-exposure baking. The CH_3 stretching and bending vibrations at 2987 cm^{-1} (peak 2) and 1372 cm^{-1} (peak 5) in the reference material and the BCPs hydrolyzed with PAG2 disappeared. Those vibrations were weaker, though still visible, in the BCPs hydrolyzed with PAG1, suggesting a lower degree of hydrolysis with PAG1 under the same conditions. For a spin-coated thin film ~50 nm in thickness, FTIR would not give a sufficient signal-to-noise ratio even in the attenuated total reflection mode. We used XRR to examine the thin films before and after photo-induced hydrolysis, where only completed hydrolysis with PAG2 gave parallel lamellae with island-hole topographies. With PAG1, the XRR profiles could be fit with a uniform monolayer after hydrolysis (Figure S9). With PAG2, the XRR profile after hydrolysis resembled the one after TFA conversion, where the reflected x-ray from the islands and holes interfered coherently (Figure S10), causing a mismatch between the experiment and simulated data from a monolayer model.

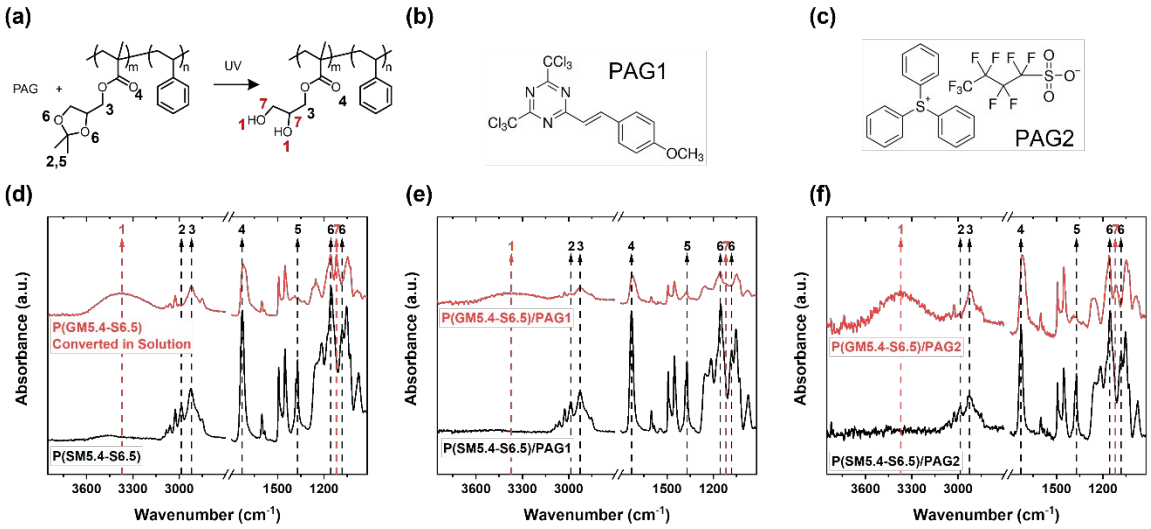

Figure 3. (a) Scheme of photo-induced hydrolysis from PSM-*b*-PS to PGM-*b*-PS. **(b)** and **(c)** Chemical structures of photoacid generator 1 (PAG1) and PAG2. **(d)** FTIR of P(SM5.4-S6.5) powders before hydrolysis and P(GM5.4-S6.5) powders after hydrolysis in solution with HCl as a catalyst. This spectrum was used as a reference for photo-induced solid-state hydrolysis. **(e)** FTIR of drop-cast film of P(SM5.4-S6.5) embedded with PAG1, with (red line) or without (black line) exposure to UV, both after baking at 100 °C. **(f)** FTIR of drop-cast film of P(SM5.4-S6.5) embedded with PAG2, with (red line) or without (black line) exposure to UV, both after baking at 100 °C. The peaks noted with red dashed arrows existed only after hydrolysis. Those numbered peaks were assigned in Figure 3(a).

For solid-state hydrolysis of thin films with PAG2, a random copolymer layer could also be used to balance interfacial interactions, promoting perpendicularly oriented cylinders, as shown in Figure 4a. PAG2 was embedded in both the random copolymer and P(SM7.6-S17.5) block copolymer layers, ensuring simultaneous hydrolysis in both layers and keeping the PGM/substrate and PS/substrate interfacial energies balanced. Compared to the hexagonally packed cylinders with lateral order obtained with PAG2, the identical BCP converted with TFA vapor followed by thermal

annealing gave poor lateral order (Figure S11). After converting PSM-*b*-PS into PGM-*b*-PS in TFA vapor, the BCPs with high χ were trapped in a metastable state with limited mobility for defect annihilation during thermal annealing. With PAG2, the acid generated during exposure to UV did not have sufficient mobility to diffuse in the film. As a result, the hydrolysis did not start until the film was placed in a solvent vapor. The lateral order evolved during solvent vapor annealing while the hydrolysis reaction proceeded simultaneously, by-passing the kinetic trapping of the high-χ BCPs, yielding high lateral order. In the AFM height image (Figure 4a), the cylinders produced by the PGM were slightly higher than the surrounding PS matrix. After rinsing the film with ethanol, a good solvent for PGM but a poor solvent for PS, the surface topography reversed, while maintaining the hexagonally packed cylindrical morphology, with the PS matrix slightly higher than the PGM cylinders. This topography change resulted from a solubilization of the PGM block and a redeposition on the surface. GISAXS (Figure S12) showed Bragg rods in the in-plane direction, confirming that the cylinders were oriented normal to the substrate. The Bragg rods resulted from the limited film thickness and a truncation of the cylinders at the substrate and surface interfaces.

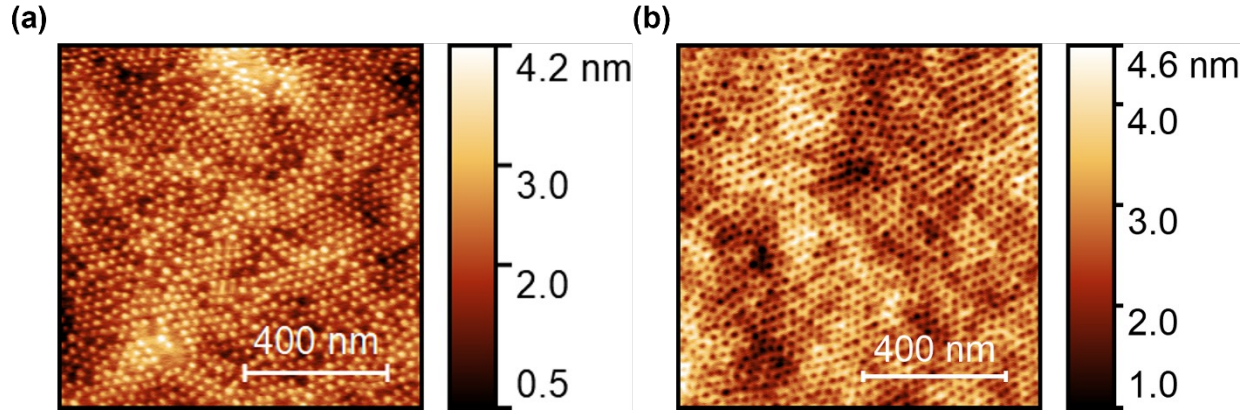

Figure 4. (a) AFM height image of P(GM7.5-S17.5) embedded with PAG2 after exposure to UV followed by solvent vapor annealing. **(b)** The same sample is shown in (a) after being rinsed with ethanol.

For linear PSM-*b*-PS, surface modifications to balance interfacial interactions are needed to promote the orientation of the lamellar microdomains normal to the film surface. Bottlebrush multiblock copolymers (Figure 5a) on the other hand, can yield this orientation without surface modification. We previously reported the synthesis and bulk self-assembly of bottlebrush (polystyrene-poly(solketal methacrylate)-polystyrene) coplymers, abbreviated as B(S-SM-S).[48] Once hydrolyzed in solution, the B(S-GM-S) is trapped in aggregated micelles. The very high χ between the PS and PGM bottlebrush blocks make it energetically unfavorable for an interpenetration of the blocks, preventing the bottlebrush copolymers from developing better lateral order. Solid-state hydrolysis on the other hand allows B(S-SM-S) to develop lateral order prior to the hydrolysis. Upon hydrolysis the PGM middle block interacts very favorably with the substrate, forcing the middle block to prient parallel to the substrate. The connectivity of the end blocks and the relative

rigidity of the bottlebrush architecture, forces the endblock to the substrate. Consequently, the microdomains orient orthogonal to the substrate surface. Confining the bottlebrush copolymers in a film thinner than a period of the lamellar microdomain morphology further promotes the ormal orientationof the microdomains. AFM height images (Figure S13) and the in-plane peaks in GISAXS (Figure S14) evidence this orientationof the micreodomains. Since PS ethes morp sloly than PGM, reactive ion etching, produced a topography that was easily discernable by scanning electron microscopy (SEM, Figure 5b). The brighter regions are the PS microdomains that protrude from the surface due to the difference in etching. This study provides an alternate strategy to orient the copolymer microdomains normal to the surface by use of the chain architecture.

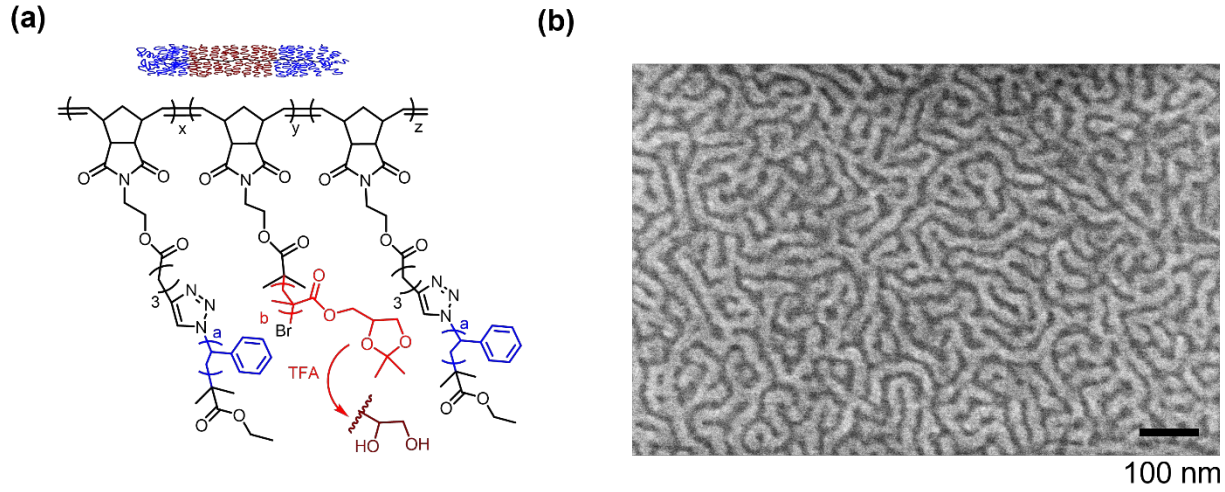

Figure 5. (a) Chemical structure of a bottlebrush triblock copolymer. Bottlebrush (polystyrene-poly(solketal methacrylate)-polystyrene) was abbreviated as B(S-SM-S). After hydrolysis of the PSM block into PGM with TFA vapor, the bottlebrush triblock copolymer was abbreviated as B(S-GM-S). (b) SEM image of the perpendicularly oriented lamellae formed with B(S-GM-S) in thin-film after TFA-induce solid-state hydrolysis, thermal annealing, and O_2/Ar reactive ion etching.

Conclusion

In this work, we obtained both lamellar and cylindrical morphologies from the self-assembly of block copolymers (BCPs) with the microdomains oriented parallel and perpendicular to the substrate. Hydrophobic-hydrophobic poly(solketal methacrylate)-block-polystyrene BCPs, were converted into hydrophilic-hydrophobic poly(glycerol monomethacrylate)-block-polystyrene BCPs in the solid state. Compared with the previously developed solid-state hydrolysis strategy where the BCPs were exposed to trifluoroacetic vapor, we developed a novel photo-induced hydrolysis strategy, where photoacid generators were embedded within the BCP thin film during spin-coating. After exposure to UV light and post-exposure baking or solvent vapor annealing, the hydrolysis reaction proceeded and transitioned the BCPs from the disordered state into the strongly microphase separated state. In addition to linear BCPs, we also explored controlling the microdomain orientation

chain architecture. Unlike linear BCPs, which require balanced interfacial interactions, the microdomains of multi-block bottlebrush copolymers can achieve the same orientation control absent any surface modification due to the strong interactions of one block with the substrate and the relttive rigidity and connectivity of the blocks. The solid state conversion of the BCP allows one to control microdomain orientation even for block with very large χ's by processing the film prior to the conversion of the BCP into the strongly phase separated state.

Acknowledgment

This work was supported by the Air Force Office of Scientific Research under contract number 21RT0488. This work benefited from the use of the SasView application, originally developed under NSF award DMR-0520547. SasView contains code developed with funding from the European Union's Horizon 2020 research and innovation program under the SINE2020 project, grant agreement No 654000. This work benefited from the *BornAgain* open-source software project, which received funding from the European Union's Horizon 2020 research and innovation program under grant agreement number 654000. This work benefited from the web-based calculator of neutron and x-ray reflectivity at https://doi.org/10.18434/M3QG67. We thank Xenocs Inc for assistance with the x-ray reflectivity measurements.

References

1. Moore, G. E., Cramming more components onto integrated circuits. Electronics: 1965; Vol. 38, pp 114-117.
2. Moore, S. K., The Node Is Nonsense. *Ieee Spectrum* **2020,** *57* (8), 25-30.
3. Bang, J.; Jeong, U.; Ryu du, Y.; Russell, T. P.; Hawker, C. J., Block copolymer nanolithography: translation of molecular level control to nanoscale patterns. *Adv Mater* **2009,** *21* (47), 4769-92.
4. Hawker, C. J.; Russell, T. P., Block copolymer lithography: Merging "bottom-up" with "top-down" processes. *Mrs Bulletin* **2005,** *30* (12), 952-966.
5. Segalman, R. A., Patterning with block copolymer thin films. *Materials Science & Engineering R-Reports* **2005,** *48* (6), 191-226.
6. Li, M. Q.; Ober, C. K., Block copolymer patterns and templates. *Materials Today* **2006,** *9* (9), 30-39.
7. Tang, C.; Lennon, E. M.; Fredrickson, G. H.; Kramer, E. J.; Hawker, C. J., Evolution of block copolymer lithography to highly ordered square arrays. *Science* **2008,** *322* (5900), 429-32.
8. Jung, Y. S.; Ross, C. A., Well-ordered thin-film nanopore arrays formed using a block-copolymer template. *Small* **2009,** *5* (14), 1654-9.
9. Jiang, X. Q.; Zhao, R. Y.; Chang, W. Y.; Yin, D. X.; Guo, Y. C.; Wang, W.; Liang, D. H.; Yang, S.; Shi, A. C.; Chen, E. Q., Highly Ordered Sub-10 nm Patterns Based on Multichain Columns of Side-Chain Liquid Crystalline Polymers. *Macromolecules* **2019,** *52* (13), 5033-5041.
10. Breaux, C. L.; Sharp, B. L.; Ludovice, P. J.; Henderson, C. L.; Li, H. B.; Li, B.; Neisser, M., Synthesis and self-assembly of high-chi poly(4-tertbutylstyrene)-block-poly(2-hydroxyethylmethacrylate). *Journal of Vacuum Science & Technology B* **2019,** *37* (1).

11. Nakatani, R.; Chandra, A.; Uchiyama, T.; Nabae, Y.; Hayakawa, T., Dynamic Ordering in High-chi Block Copolymer Lamellae Based on Cross-Sectional Orientational Alignment. *ACS Macro Lett* **2019,** *8* (9), 1122-1127.
12. Cushen, J. D.; Bates, C. M.; Rausch, E. L.; Dean, L. M.; Zhou, S. X.; Willson, C. G.; Ellison, C. J., Thin Film Self-Assembly of Poly(trimethylsilylstyrene-b-D,L-lactide) with Sub-10 nm Domains. *Macromolecules* **2012,** *45* (21), 8722-8728.
13. Cushen, J. D.; Otsuka, I.; Bates, C. M.; Halila, S.; Fort, S.; Rochas, C.; Easley, J. A.; Rausch, E. L.; Thio, A.; Borsali, R.; Willson, C. G.; Ellison, C. J., Oligosaccharide/silicon-containing block copolymers with 5 nm features for lithographic applications. *ACS Nano* **2012,** *6* (4), 3424-33.
14. Kennemur, J. G.; Yao, L.; Bates, F. S.; Hillmyer, M. A., Sub-5 nm Domains in Ordered Poly(cyclohexylethylene)-block-poly(methyl methacrylate) Block Polymers for Lithography. *Macromolecules* **2014,** *47* (4), 1411-1418.
15. Cushen, J.; Wan, L.; Blachut, G.; Maher, M. J.; Albrecht, T. R.; Ellison, C. J.; Willson, C. G.; Ruiz, R., Double-Patterned Sidewall Directed Self-Assembly and Pattern Transfer of Sub-10 nm PTMSS-b-PMOST. *ACS Appl Mater Interfaces* **2015,** *7* (24), 13476-83.
16. Otsuka, I.; Zhang, Y.; Isono, T.; Rochas, C.; Kakuchi, T.; Satoh, T.; Borsali, R., Sub-10 nm Scale Nanostructures in Self-Organized Linear Di- and Triblock Copolymers and Miktoarm Star Copolymers Consisting of Maltoheptaose and Polystyrene. *Macromolecules* **2015,** *48* (5), 1509-1517.
17. Kwak, J.; Mishra, A. K.; Lee, J.; Lee, K. S.; Choi, C.; Maiti, S.; Kim, M.; Kim, J. K., Fabrication of Sub-3 nm Feature Size Based on Block Copolymer Self-Assembly for Next-Generation Nanolithography. *Macromolecules* **2017,** *50* (17), 6813-6818.
18. Lane, A. P.; Yang, X.; Maher, M. J.; Blachut, G.; Asano, Y.; Someya, Y.; Mallavarapu, A.; Sirard, S. M.; Ellison, C. J.; Willson, C. G., Directed Self-Assembly and Pattern Transfer of Five Nanometer Block Copolymer Lamellae. *ACS Nano* **2017,** *11* (8), 7656-7665.
19. Li, X. M.; Li, J.; Wang, C. X.; Liu, Y. Y.; Deng, H., Fast self-assembly of polystyrene-b-poly(fluoro methacrylate) into sub-5 nm microdomains for nanopatterning applications. *Journal of Materials Chemistry C* **2019,** *7* (9), 2535-2540.
20. Sun, J.; Lee, C.; Osuji, C. O.; Gopalan, P., Synthesis of High Etch Contrast Poly(3-hydroxystyrene)-Based Triblock Copolymers and Self-Assembly of Sub-5 nm Features. *Macromolecules* **2021,** *54* (20), 9542-9550.
21. Li, D. X.; Chien, C. L.; Wei, X. N.; Huang, Y. W.; Qu, X. P.; Chang, T. H.; Xiong, S. S. In *Sub-10 nm silicon FinFET devices on SOI substrate made by block copolymer lithography*, 14th IEEE International Conference on Solid-State and Integrated Circuit Technology (ICSICT), Qingdao, PEOPLES R CHINA, Oct 31-Nov 03; Qingdao, PEOPLES R CHINA, 2018; pp 21-23.
22. Liu, C. C.; Franke, E.; Mignot, Y.; Xie, R. L.; Yeung, C. W.; Zhang, J. Y.; Chi, C.; Zhang, C.; Farrell, R.; Lai, K. F.; Tsai, H.; Felix, N.; Corliss, D., Directed self-assembly of block copolymers for 7 nanometre FinFET technology and beyond. *Nature Electronics* **2018,** *1* (10), 562-569.
23. Galatsis, K.; Wang, K. L.; Ozkan, M.; Ozkan, C. S.; Huang, Y.; Chang, J. P.; Monbouquette, H. G.; Chen, Y.; Nealey, P.; Botros, Y., Patterning and templating for nanoelectronics. *Adv Mater* **2010,** *22* (6), 769-78.
24. Pound-Lana, G.; Bezard, P.; Petit-Etienne, C.; Cavalaglio, S.; Cunge, G.; Cabannes-Boue, B.; Fleury, G.; Chevalier, X.; Zelsmann, M., Dry-Etching Processes

for High-Aspect-Ratio Features with Sub-10 nm Resolution High-chi Block Copolymers. *ACS Appl Mater Interfaces* **2021,** *13* (41), 49184-49193.
25. Bates, F. S.; Fredrickson, G. H., Block copolymers - Designer soft materials. *Physics Today* **1999,** *52* (2), 32-38.
26. Leibler, L., Theory of Microphase Separation in Block Co-Polymers. *Macromolecules* **1980,** *13* (6), 1602-1617.
27. Bates, F. S.; Fredrickson, G. H., Block copolymer thermodynamics: theory and experiment. *Annu Rev Phys Chem* **1990,** *41*, 525-57.
28. Ren, Y.; Lodge, T. P.; Hillmyer, M. A., Effect of selective perfluoroalkylation on the segregation strength of polystyrene - 1,2-polybutadiene block copolymers. *Macromolecules* **2002,** *35* (10), 3889-3894.
29. Liu, F.; Goldenfeld, N., Dynamics of phase separation in block copolymer melts. *Phys Rev A Gen Phys* **1989,** *39* (9), 4805-4810.
30. Sinturel, C.; Bates, F. S.; Hillmyer, M. A., High chi-Low N Block Polymers: How Far Can We Go? *ACS Macro Lett* **2015,** *4* (9), 1044-1050.
31. Durand, W. J.; Blachut, G.; Maher, M. J.; Sirard, S.; Tein, S.; Carlson, M. C.; Asano, Y.; Zhou, S. X.; Lane, A. P.; Bates, C. M.; Ellison, C. J.; Willson, C. G., Design of High-chi Block Copolymers for Lithography. *J Polym Sci Pol Chem* **2015,** *53* (2), 344-352.
32. Jennings, J.; Cornel, E. J.; Derry, M. J.; Beattie, D. L.; Rymaruk, M. J.; Deane, O. J.; Ryan, A. J.; Armes, S. P., Synthesis of High chi-Low N Diblock Copolymers by Polymerization-Induced Self-Assembly. *Angew Chem Int Ed Engl* **2020,** *59* (27), 10848-10853.
33. Yu, D. M.; Smith, D. M.; Kim, H.; Mapas, J. K. D.; Rzayev, J.; Russell, T. P., Morphological Evolution of Poly(solketal methacrylate)-block-polystyrene Copolymers in Thin Films. *Macromolecules* **2019,** *52* (10), 3592-3600.
34. Scheurer, M.; Nodler, K., Ultrashort-chain perfluoroalkyl substance trifluoroacetate (TFA) in beer and tea - An unintended aqueous extraction. *Food Chem* **2021,** *351*, 129304.
35. Shin, C.; Ahn, H.; Kim, E.; Ryu, D. Y.; Huh, J.; Kim, K. W.; Russell, T. P., Transition Behavior of Block Copolymer Thin Films on Preferential Surfaces. *Macromolecules* **2008,** *41* (23), 9140-9145.
36. Bates, C. M.; Seshimo, T.; Maher, M. J.; Durand, W. J.; Cushen, J. D.; Dean, L. M.; Blachut, G.; Ellison, C. J.; Willson, C. G., Polarity-switching top coats enable orientation of sub-10-nm block copolymer domains. *Science* **2012,** *338* (6108), 775-9.
37. Wang, H. S.; Kim, K. H.; Bang, J., Thermal Approaches to Perpendicular Block Copolymer Microdomains in Thin Films: A Review and Appraisal. *Macromol Rapid Commun* **2019,** *40* (4), e1800728.
38. Suh, H. S.; Kim, D. H.; Moni, P.; Xiong, S.; Ocola, L. E.; Zaluzec, N. J.; Gleason, K. K.; Nealey, P. F., Sub-10-nm patterning via directed self-assembly of block copolymer films with a vapour-phase deposited topcoat. *Nat Nanotechnol* **2017,** *12* (6), 575-581.
39. Li, J. J.; Zhou, C.; Chen, X. X.; Delgadillo, P. A. R.; Nealey, P. F., Orientation control of high-chi triblock copolymer for sub-10 nm patterning using fluorine-containing polymeric additives. *Journal of Micro-Nanolithography Mems and Moems* **2019,** *18* (3).
40. Oh, J.; Shin, M.; Kim, I. S.; Suh, H. S.; Kim, Y.; Kim, J. K.; Bang, J.; Yeom, B.; Son, J. G., Shear-Rolling Process for Unidirectionally and Perpendicularly Oriented

Sub-10-nm Block Copolymer Patterns on the 4 in Scale. *ACS Nano* **2021,** *15* (5), 8549-8558.
41. Singh, M.; Agrawal, A.; Wu, W.; Masud, A.; Armijo, E.; Gonzalez, D.; Zhou, S.; Terlier, T.; Zhu, C.; Strzalka, J.; Matyjaszewski, K.; Bockstaller, M.; Douglas, J. F.; Karim, A., Soft-Shear-Aligned Vertically Oriented Lamellar Block Copolymers for Template-Free Sub-10 nm Patterning and Hybrid Nanostructures. *ACS Appl Mater Interfaces* **2022,** *14* (10), 12824-12835.
42. Hu, M.; Russell, T. P., Polymers with advanced architectures as emulsifiers for multi-functional emulsions. *Materials Chemistry Frontiers* **2021,** *5* (3), 1205-1220.
43. Rokhlenko, Y.; Kawamoto, K.; Johnson, J. A.; Osuji, C. O., Sub-10 nm Self-Assembly of Mesogen-Containing Grafted Macromonomers and Their Bottlebrush Polymers. *Macromolecules* **2018,** *51* (10), 3680-3690.
44. Gu, W.; Huh, J.; Hong, S. W.; Sveinbjornsson, B. R.; Park, C.; Grubbs, R. H.; Russell, T. P., Self-assembly of symmetric brush diblock copolymers. *ACS Nano* **2013,** *7* (3), 2551-8.
45. Hong, S. W.; Gu, W.; Huh, J.; Sveinbjornsson, B. R.; Jeong, G.; Grubbs, R. H.; Russell, T. P., On the self-assembly of brush block copolymers in thin films. *ACS Nano* **2013,** *7* (11), 9684-92.
46. Yu, D. M.; Mapas, J. K. D.; Kim, H.; Choi, J.; Ribbe, A. E.; Rzayev, J.; Russell, T. P., Evaluation of the Interaction Parameter for Poly(solketal methacrylate)-block-polystyrene Copolymers. *Macromolecules* **2018,** *51* (3), 1031-1040.
47. Jeong, G.; Yu, D. M.; Mapas, J. K. D.; Sun, Z. W.; Rzayev, J.; Russell, T. P., Realizing 5.4 nm Full Pitch Lamellar Microdomains by a Solid-State Transformation. *Macromolecules* **2017,** *50* (18), 7148-7154.
48. Hu, M.; Li, X.; Rzayev, J.; Russell, T. P., Hydrolysis-Induced Self-Assembly of High-χ–Low-N Bottlebrush Copolymers. *Macromolecules* **2021,** *54* (24), 11449-11458.
49. Chen, Z.; Hu, M.; Li, X.; Smith, D. M.; Seong, H. G.; Emrick, T.; Rzayev, J.; Russell, T. P., In Situ Hydrolysis of Block Copolymers at the Water-Oil Interface. *Angew Chem Int Ed Engl* **2022,** *61* (25), e202201392.
50. http://www.sasview.org/.
51. Guinier, A.; Fournet, G.; Yudowitch, K. L., Small-angle scattering of X-rays. **1955**.
52. Russell, T. P., X-ray and neutron reflectivity for the investigation of polymers. *Materials Science Reports* **1990,** *5* (4), 171-271.
53. Pospelov, G.; Van Herck, W.; Burle, J.; Carmona Loaiza, J. M.; Durniak, C.; Fisher, J. M.; Ganeva, M.; Yurov, D.; Wuttke, J., BornAgain: software for simulating and fitting grazing-incidence small-angle scattering. *J Appl Crystallogr* **2020,** *53* (Pt 1), 262-276.
54. Maranville, B. B., Interactive, Web-Based Calculator of Neutron and X-ray Reflectivity. *J Res Natl Inst Stand Technol* **2017,** *122*, 1-6.
55. Pavia, D. L.; Lampman, G. M.; Kriz, G. S.; Vyvyan, J. A., *Introduction to spectroscopy*. Cengage learning: 2014.
56. Kyeremateng, S. O.; Amado, E.; Kressler, J., Synthesis and characterization of random copolymers of (2,2-dimethyl-1,3-dioxolan-4-yl)methyl methacrylate and 2,3-dihydroxypropyl methacrylate. *European Polymer Journal* **2007,** *43* (8), 3380-3391.